sustainability

MDPI

Article

Study on the Evolutionary Characteristics of Acoustic–Magnetic–Electric Signals in the Entire Process of Coal and Gas Outburst

Jianchun Ou [1], Enyuan Wang [2,*], Zhonghui Li [2], Nan Li [1], He Liu [2] and Xinyu Wang [2]

[1] State Key Laboratory for Fine Exploration and Intelligent Development of Coal Resources, China University of Mining and Technology, Xuzhou 221116, China
[2] School of Safety Engineering, China University of Mining and Technology, Xuzhou 221116, China
* Correspondence: eywangcumt@163.com

Abstract: In recent years, with the continuous increase in the depth and intensity of coal mining, coal and gas outburst disasters pose a severe threat to the safe production of coal mines. Thus, this experiment studied the characteristics of electromagnetic radiation, acoustic emission, and electric potential signals during gas adsorption, stress loading, and the entire outburst process. The results indicate that during the adsorption process, different parts of the coal body exhibit variations in electric potential signals, electromagnetic radiation, and acoustic emissions. During the loading process, the consistency between the acoustic–electric signals and the load change rate is good, and at the moment of outburst, the acoustic–electric signals significantly increase with the ejection of coal and gas. Outbursts generally occur during the decline in electromagnetic radiation and acoustic emission signals, with the internal electric potential signal strength first decreasing then rapidly increasing and the surface electric potential directly rising. The closer to the outburst opening, the greater the change in signal amplitude. Based on the above experimental results, the outburst can be monitored through the acoustic–magnetic–electric precursory signal changes during the adsorption and loading processes, which is of great significance to the safety production and rapid excavation of coal mines.

Keywords: coal and gas outburst; acoustic emission; electromagnetic radiation; electric potential; spatiotemporal evolution

check for updates

Citation: Ou, J.; Wang, E.; Li, Z.; Li, N.; Liu, H.; Wang, X. Study on the Evolutionary Characteristics of Acoustic–Magnetic–Electric Signals in the Entire Process of Coal and Gas Outburst. *Sustainability* **2023**, *15*, 15944. https://doi.org/10.3390/su152215944

Academic Editor: Chaolin Zhang

Received: 28 September 2023
Revised: 1 November 2023
Accepted: 2 November 2023
Published: 14 November 2023

Copyright: © 2023 by the authors. Licensee MDPI, Basel, Switzerland. This article is an open access article distributed under the terms and conditions of the Creative Commons Attribution (CC BY) license (https://creativecommons.org/licenses/by/4.0/).

1. Introduction

As the demand for coal resources in China is large, and the shallow coal resources are gradually depleting with lower economic value, deep mining has become the main area of coal mining in China [1,2]. In recent years, with the continuous increase in the depth and intensity of coal mining, the intensity and frequency of disasters have increased [3,4]. Coal and gas outbursts are a complex dynamic disaster phenomenon in the coal mining process [5] that can instantly emit a large amount of coal and gas into tunnels, mining faces, and other excavated spaces. Coal and gas outbursts not only pose a serious threat to mine safety production but also lead to a massive waste of resources. At the same time, the outburst releases a large amount of greenhouse gases such as methane, causing atmospheric pollution and exacerbating global climate change. This severely violates the requirements for efficient resource use and environmental protection in sustainable development [6,7]. Therefore, it is crucial to conduct scientific research to thoroughly understand the causes and mechanisms of coal and gas outbursts and to formulate effective prevention and control strategies, in order to reduce the frequency and impact of such disasters, ensure the rational use of coal mine resources, and alleviate their negative effects on the environment, as this is key to advancing sustainable development [8]. During the process of coal and gas outbursts, changes in the coal structure and surrounding environment release acoustic emission (AE)

signals, electromagnetic radiation (EMR), electric potential (EP) signals, and there are significant changes in the gas pressure of the coal seam [9]. Therefore, by combining the monitoring of EMR, AE signals, and EP signals, accurate monitoring and early warning of coal and rock dynamic disasters can be achieved, thereby significantly reducing the risk of coal and gas outbursts [10,11].

Due to the suddenness, danger, and concealment of outbursts, directly studying the occurrence and mechanism of outbursts at the coal mine site is difficult and hazardous. Therefore, laboratory testing is an effective research method, and many researchers have conducted extensive studies on the early warning of coal and gas outbursts using laboratory simulation means. Soleimani et al. [12] conducted 3D numerical simulations to study outburst initiation in a coal seam during roadway development, calculating the energies involved to pinpoint the precise moment of outburst initiation. The results reveal a direct correlation between the damaged zone volume and outburst intensity; an outburst is probable when more than 6% of the remaining coal ahead of the face reaches the maximum damage variable. Yin et al. [13] developed a large-scale coal and gas outburst simulation experimental device to address the shortcomings of small-scale simulation experimental devices. It can accommodate large coal samples with different coal seam angles and outburst intensities under different ground stresses and gas pressures, and both uniform and non-uniform load distributions can be applied to the coal samples. Such a loading system can simulate the local concentration of stress, further improving the reliability and accuracy of the simulation experiments. Li et al. [14] used self-developed continuous monitoring and early warning equipment for acoustic emissions to monitor and predict dynamic disasters of coal and gas outbursts at the working face. The results showed that AE had a significant rising trend before the accident occurred and preceded the change in gas concentration; the AE can provide advanced warning for coal-rock gas dynamic disasters. Many scholars have achieved certain results in the research of coal and gas outbursts. Among them, EMR [15] and AE [16–18] technologies, as non-contact prediction methods, have the advantages of not requiring drilling, not occupying production time, and being able to achieve a continuous prediction of outburst danger. They have been widely used in coal and gas early warning technology and have achieved certain effects. Based on acoustic and electric emission signals, real-time continuous monitoring of the stress state and fracture process of the coal body can be realized [19]. Zhang et al. [16] used a self-developed true triaxial coal and gas outburst simulation device to simulate coal and gas outbursts at different depths. From the perspective of AE energy, they defined quantitative indicators reflecting the breeding risk of coal and gas outbursts. The ratio of the average AE energy in the later incubation and the early incubation is defined as L_1, and the ratio of the high energy frequency to the low energy frequency is defined as L_2. When $L_1 < 5.0$, $L_2 < 0.3$, it is in the early incubation with a weak outburst risk. When $L_1 > 5.0$, $L_2 > 2.2$, it is in the later incubation with a strong outburst risk. Qiu et al. [20] conducted a mechanical analysis of the dynamic manifestation process of three typical coal and gas outbursts in the 14141 working face of the Jiulishan coal mine through EMR, which resulted in the strong connection between EMR signals and the alterations in stress, fracturing, and gas flow during mining, noting that heightened outburst risks lead to distinguishable changes in the EMR signal across both time and frequency domains. Specifically in the time domain, there is a direct correlation between EMR intensity and the outburst danger of the coal seam, with the EMR intensity's variable coefficient surpassing 0.15 during dynamic occurrences and its peak value being indicative of the coal local instability.

Both AE and EMR technologies have been commercialized, and many scholars have achieved significant results in the study of coal and gas outbursts through AE and EMR technologies [21–25]. However, the current research mainly focuses on the development phase of outbursts, and there are certain shortcomings in the study of the entire outburst process. The precursor characteristics of the EMR and AE signals are not entirely clear. Moreover, coal mining activities can easily interfere with signals, and it is difficult to

accurately predict based solely on AE or EMR analysis [26]. With the further development of monitoring methods, researchers found that under the coupled effects of loading stress and gas pressure, an EP signal is produced during the deformation and damage process of the coal body, and the response characteristics of the EP signal are closely related to the loading state and damage evolution process of the coal body [27]. Liu et al. [28], Niu et al. [29], and Qiu et al. [30] systematically explored the characteristics, laws, and mechanisms of the coal-rock EP effect and conducted preliminary field experiments and applications. The results show that the abnormal time series response characteristics of EP can be regarded as a precursor to coal body damage under the coupled effects of stress and gas. At the same time, EP signals are not only sensitive to large-scale coal body rupture events [31] but also respond to coal body deformation, revealing in-depth the damage evolution process of gas-containing coal bodies [32].

A substantial amount of work has already been carried out on the study of AE, EMR, and EP signals in coal and gas outbursts [33,34]. However, the research mainly focuses on the outburst phase, and there is still some inadequacy in the study of the entire process. The complex structure of the coal mass affects the transmission and accuracy of signals, and the previous studies only considered the signal patterns of single monitoring methods. There is a lack of comprehensive analysis of the precursor patterns of AE-EMR-EP signals. A reasonable comprehensive analysis of AE-EMR-EP signals will greatly improve the accuracy and timeliness of monitoring and early warning. In this paper, the outburst simulation experiment was conducted based on a self-developed tunneling outburst simulation system. The AE, EMR, and EP signals during the gas adsorption process, loading process, and outburst process were thoroughly studied. This has significant practical implications for enhancing the accuracy of coal and gas outburst early warning and ensuring safe coal mining operations.

2. Experimental Method

Qiu et al. [30] utilized a self-developed experimental system mainly consisting of a loading system, AE-EMR data acquisition system, and interference shielding system. It conducted uniaxial compression tests on coal samples, collecting and processing AE and EMR signals from the specimens. Niu et al. [35] developed an EP meter comprised of a mainframe, testing electrodes, shielded cables, and a remote control. It collected EP data from arranged measurement points in the field tunnels, comparing it with conventional tests. Due to the hazardous nature of the field and the lengthy cycles of on-site testing, this experiment utilized laboratory simulation methods for testing, concurrently recording AE, EMR, and EP signals.

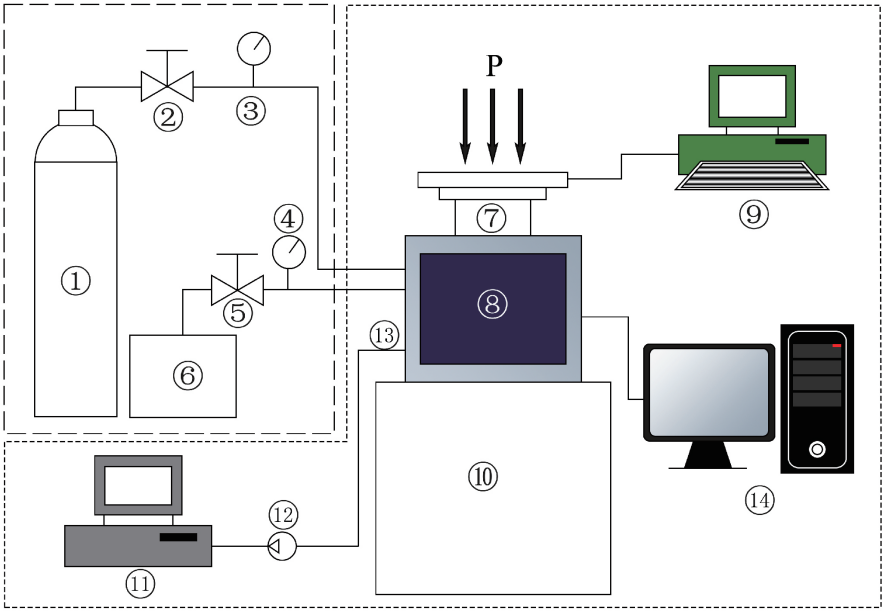
2.1. Specimen Preparation

Since briquette coal is an ideal substitute for raw coal in the coal-rock loading experiment process [35], it was used as the sample in this experiment. The original coal sample for the experiment was taken from Jiulishan Coal Mine of Jiaozuo Mining Bureau, and the briquette coal was prepared using on-site soft stratification, sealed after on-site sampling, and crushed to a granularity below 1 mm in the laboratory. The briquette coal was directly pre-made in the outburst experimental device. The well-proportioned coal powder was loaded into the experimental device in three batches, compressed each time it was added, with a pressure value of 20 MPa. The press was controlled to load at a rate of 300 N/s when pre-making briquette coal, and it was maintained for 30 min after reaching the predetermined pressure. Before the briquette coal is compressed, the outburst opening is sealed, and the pre-made briquette coal is fully combined with the container wall.

2.2. Test System

The experimental apparatus is shown in Figure 1, including a pressure loading device, gas loading device, outburst initiation device, landing device, and data collection and analysis device. The pressure loading device consists of a microcomputer-controlled electro-

hydraulic servo pressure testing machine. Loading system: YAW4306 microcomputer-controlled electro-hydraulic servo pressure testing machine (Xuzhou, China). The testing machine has a maximum load of 3000 kN, a test force indication resolution (FS) of 1/300,000, a relative error of the test force indication of ±1% of the indication value, a loading rate of 600∼60,000 N/s, a loading rate accuracy of ±1%, and employs both force and displacement control methods. It can perform uniaxial compression, tension, cyclic loading, creep, and other tests. The data collection and analysis device is used to collect various signal features during the coal and gas outburst experiment process. The surface potential data are collected using the LB-IV type multi-channel potential data acquisition system. The LB-IV type multi-channel potential data acquisition system mainly consists of a central controller, data collector, and front-end bridge amplifier. This instrument is equipped with 16 acquisition channels, which can be used simultaneously to connect copper sheet electrodes and strain gauges for measuring surface potential or strain during the deformation and fracture process of coal and rock, with a 16-bit A/D conversion resolution. The sampling frequency is up to 100 Hz for continuous acquisition and up to 1000 Hz for fixed-length (200 s) acquisition. EMR and AE data collection use the CTA-1 type acoustic and electric dynamic data acquisition system. The arrangement method of the potential, EMR, and AE sensors used in the experiment is shown in Figure 2a, where channels 1, 5, and 6 are EMR sensors, and channels 2, and 8 are AE sensors; the arrangement of potential sensors is shown in Figure 2b, where 2, 4, and 11 are internal potentials, and 3, 5, 6, 7, and 8 are surface potentials.



1	gas cylinder	8	coal sample
2	pressure reducing valve	9	load control system
3	pressure gauge	10	Microcomputer controlled electro-hydraulic servo pressure testing machine
4	vacuum gauge	11	data collection system
5	vacuum control valve	12	preamplifier
6	vacuum pump	13	sensor
7	piston	14	data collection system

Figure 1. Schematic Diagram of the Experimental Device.

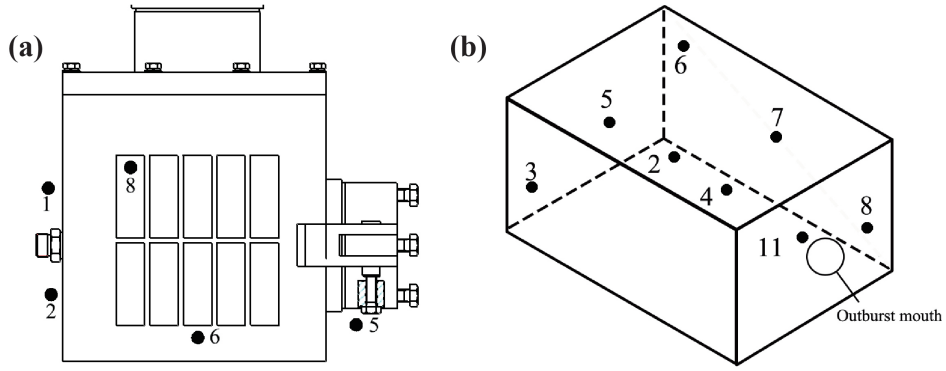


Figure 2. Layout of acousto-electric sensors (**a**) and layout of potential measurement points (**b**).

2.3. Test Procedures

(1) Preparation and System Airtightness Check: Seal the experimental device securely. Use a vacuum pump to evacuate the experimental device and ensure its airtightness.
(2) Gas Adsorption Process: Use the gas loading module to inflate the coal sample under constant pressure for 24 h to achieve adsorption equilibrium.
(3) Pressure Application and Signal Collection Setup: Utilize a servo press to apply pressure onto the coal sample, matching the required load pressure with the actual stress conditions in the mine (approximately 10 MPa for a coal sample buried 430 m deep). Initiate the signal collection system to continuously gather and record signals throughout the entire duration of the experiment.
(4) Simulation of Coal Roadway Excavation and Induction of Coal and Gas Outbursts: Employ a hot air gun to heat and melt paraffin, altering the power of the gun to simulate changes in the advancement speed of a coal roadway.
(5) Data Processing: Apply the load to the specimen using the press to synchronously measure various data such as EP, EMR, and AE.
(6) After finishing the test, turn off all test systems in turn.

3. Results and Discussion

In this section, utilizing the self-developed outburst simulation experimental system, a substantial number of coal and gas outburst simulation experiments were conducted. We observed in real-time the patterns of AE, EMR, and EP signals during the adsorption phase, loading phase, and outburst phase of the experiments, and through the analysis of the regularities of coal and gas outbursts, provided a theoretical basis for the further field application of AE-EMR-EP signals in predicting coal and gas outburst.

3.1. The Characteristic of AE, EMR, and EP Signals during the Gas Adsorption Process

As illustrated in Figure 3, the time span from 0 to 8000 s indicates the variations in EMR and AE signals during the gas injection process. Overall, the EMR produced by the coal body tends to increase with the rise of gas pressure. The data from channels 1, 5, and 6 indicate that after gas injection began, the EMR signal showcased an upward trend with the rise in gas pressure in the coal sample. Around 700 s, the EMR signal intensity peaked. The emergence of EMR could be attributed to the deformation of the coal matrix due to the gas, leading to coal fractures. The subsequent phase indicates a stable adsorption period where the EMR signals remain relatively consistent. Near the end of the gas injection, at around 8000 s, there was a sudden surge in signal pulses when the valve was abruptly closed.

The process of coal adsorbing gas, or the migration of gas within the coal, is a typical flow–solid coupling process involving adsorption [36]. Within this process, the stress induced by coal adsorbing gas could result in damages to the coal's micro and mesoscopic

structures, thereby releasing energy. AE indicates the fracturing or extension of pre-existing flaws or damages in the coal-rock mass [37]. Structural changes in the coal-rock mass release energy rapidly in the form of elastic waves. The AE of the coal-rock mass reflects the internal damage degree, which is directly associated with its internal flaw or damage evolution [30]. The AE signals produced by the coal body during the gas adsorption process can be attributed to two factors. On the one hand, gas adsorption causes the coal matrix to swell and deform, leading to micro-deformations or micro-fractures in the coal structure, generating AE signals. On the other hand, the existing pressure gradient within the coal body can cause stretching or shearing fractures, producing AE signals [10,38]. On the microscopic level, the adsorption of gas by coal leads to the expansion of the coal matrix, resulting in minor deformations or fractures. The surface of the coal matrix has a reduction in adsorption potential, gas molecules are adsorbed by the coal, reducing the surface free energy of the coal, causing expansion, and the greater the amount of gas adsorbed, the greater the reduction in surface energy, leading to increased deformation of the coal matrix. At the same time, the infiltration of gas into the coal matrix can generate additional expansive stress, causing damage to the microscopic structure of the coal. On the mesoscopic level, the gas pressure gradient can damage the microscopic structure of the coal matrix. The gas pressure gradient is the direct cause of coal matrix damage, and an increase in the gas pressure gradient can lead to an increase in effective tensile stress [39].

When the gas pressure gradient is sufficiently large, it causes damage to the coal matrix, and the characteristic length of layer cracking is closely related to the gas seepage and the tensile strength of the coal matrix. This indicates that there exists a critical gas pressure gradient that can cause damage to the microscopic structure of the coal matrix, and this critical value is closely related to the tensile strength of the coal matrix, as shown in Equation (1).

$$\text{grad}\, P \geq K_i \tag{1}$$

where grad P represents the gas pressure gradient, and K_i represents the critical pressure gradient that can cause damage to the coal matrix.

In the experiment, the gas pressure used is constant, but the gas pressure gradient in the coal matrix also depends on the length. Although the gas pressure is small in the experiment, a higher gas pressure gradient can still be formed in local minor segments, thereby causing damage to the microporous structure in the coal matrix. As the process of gas adsorption and seepage in the coal matrix is a layer-by-layer penetration process, gas always first breaks through areas of lower strength within the coal matrix. At the same time, due to the maximum gas pressure gradient at the initial stage of the experiment, a peak of AE signals generally appears at the beginning of the experiment. After the coal matrix structure undergoes damage due to the action of the gas, the gas pressure at the seepage front drops sharply, and the gas pressure is not sufficient to overcome coal matrix units with higher strength, while gas seepage enters the energy storage stage. When the gas pressure gradually increases with the adsorption time to form a higher gas pressure gradient, a second peak of AE signals appears in the coal matrix.

During the adsorption process, the characteristic behavior of AE signals is also affected by the homogeneity of the coal matrix. As the experiment uses large-scale coal samples, which are different from the standard coal samples used in ordinary experiments, the heterogeneity of the large-scale coal samples is more pronounced, having a greater impact on the experimental results. Due to the heterogeneity of the coal matrix, the strength varies in different parts of it, which also intensifies the irregularity of the AE signals during the coal matrix layer seepage process.

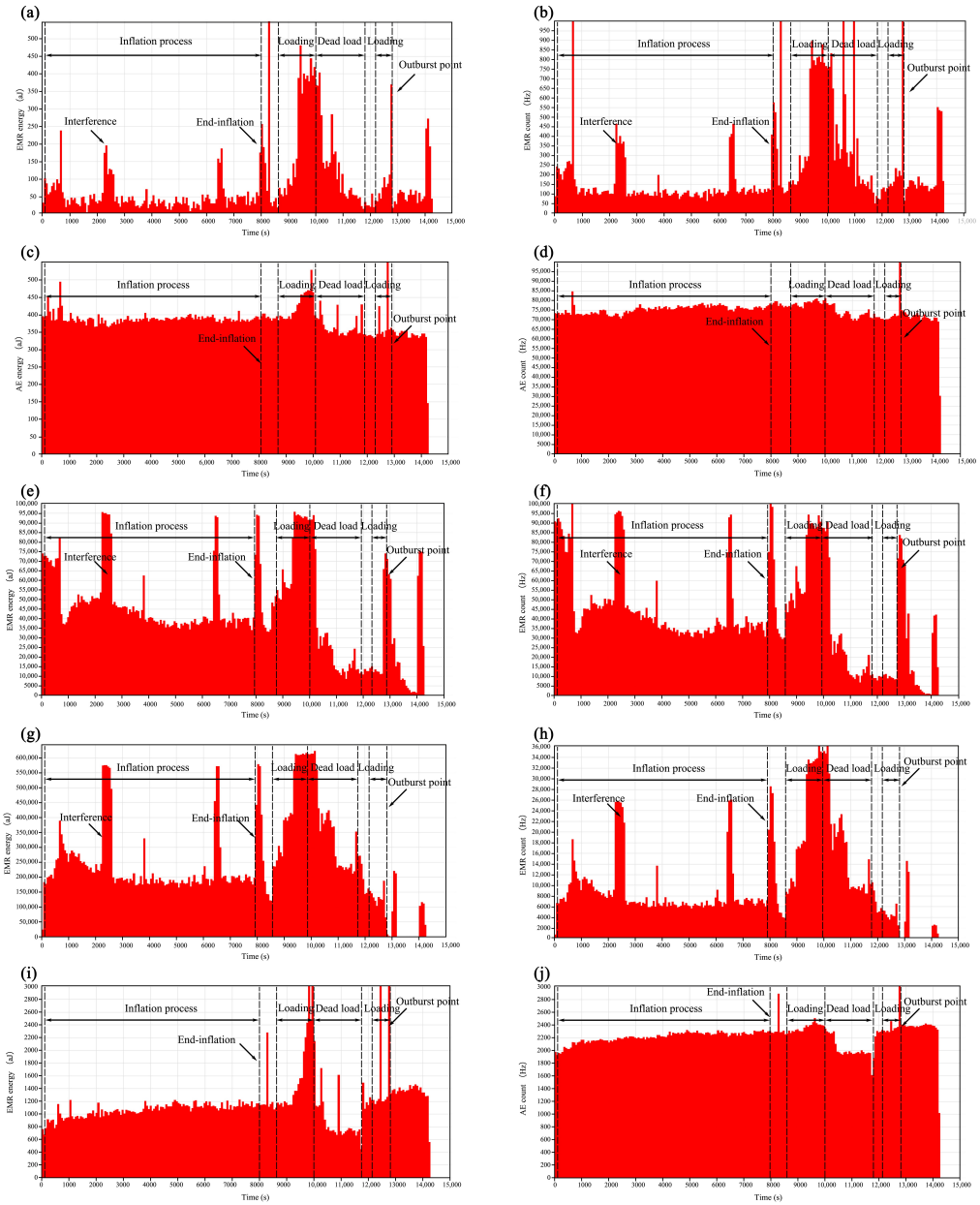


Figure 3. The test results of the coal sample gas charging process (0.32 MPa), Channel 1 EMR energy (**a**) and count (**b**) (50 KHz), Channel 2 AE energy (**c**) and count (**d**) (57.16 KHz), Channel 5 EMR energy (**e**) and count (**f**) (25 KHz), Channel 6 EMR energy (**g**) and count (**h**) (25 KHz), Channel 8 AE energy (**i**) and count (**j**) (20 KHz).

Figure 4 illustrates the variation in the EP signal throughout the entire experimental process. EP signals are produced from the deformation and failure of the coal rock, simultaneously with EMR. Raw coal, rocks, and other materials generate potential, free electric charge, and resistivity under the load. Based on the physical mechanism, processes such as friction, charge separation caused by crack propagation, external electron emission from crack tips, and stress induction can all induce a potential response [35]. From the perspective of engineering applications, the change in EP signal can be regarded as caused by the sudden change in the stress state and distribution, as well as the deformation and failure of the coal-rock mass. The EP signal often experiences abrupt changes and exhibits other response characteristics before or after the main fracture of the coal-rock sample occurs. The increase or decrease in EP signal is closely related to the stress state and failure process of coal and rock materials. More importantly, the EP response has the advantages of high

sensitivity and strong anti-interference. At the beginning of the gas charging phase until around 700 s, the intensity of the electrical potential signal starts to decrease. After a brief period of signal enhancement, the electrical potential signal exhibits a weakening trend.

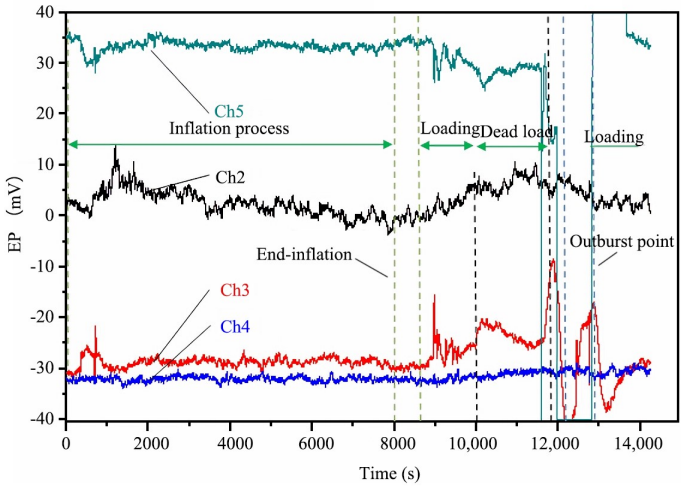


Figure 4. The electrical potential test results during the coal sample gas charging process at Jiulishan Mine, Jiaozuo (0.32 MPa).

3.2. The Characteristics of the AE, EMR, and EP Signals during the Loading Process

In Figure 3, the period from 8750 s to 11,750 s corresponds to the acoustic–electric signals during the loading process. The stress–strain curve during loading is shown in Figure 5. In this stage, loading is divided into two phases: loading and constant load. The range from 8750 s to 10,000 s represents the loading phase, while 10,000 s to 11,750 s represents the constant load phase. From Figure 3, it can be observed that during the loading phase, there is good consistency between the EMR signals, AE signals, and the variation in the load as stress increases. During the constant load phase from 10,000 s to 11,750 s, both EMR and AE signals decrease. In this phase, the force within the coal matrix remains constant, meaning the rate of the load change is zero. During this phase, the acoustic–electric signals are weaker, indicating good consistency between EMR, acoustic emission and the rate of force change. From 12,200 s to 12,800 s, the second loading phase on the coal matrix is observed. As stress increases, the acoustic–electric signals intensify, but the amplitude is much smaller compared to the first loading phase.

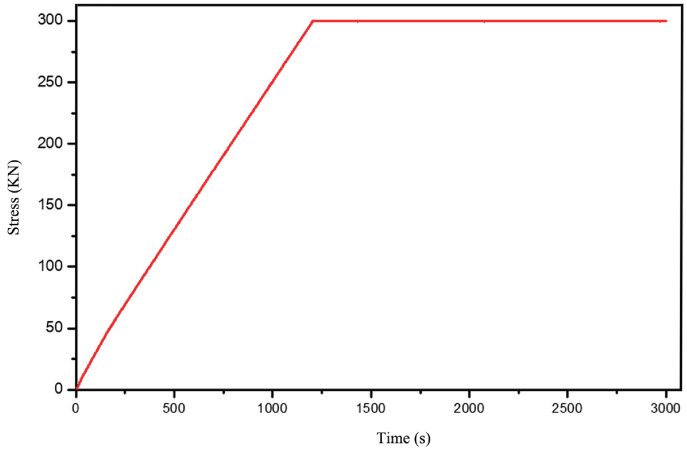


Figure 5. The stress–strain curve during the loading process.

There is a correlation between EMR, AE, and the rheological damage of coal. The intensity of EMR and AE signals increases with the increase in stress and the degree of coal deformation and fracture. It also increases with increased stress level, stress loading rate, and deformation rate [35]. Figure 6 shows the results of acoustic–electric testing during the loading process. From the graph, it can be observed that overall, EMR and AE increase with the increasing stress as loading progresses. Channel 5 in Figure 5 represents the AE data. From the data pattern, several points with significant changes in AE signals correspond to sudden changes in loading speed, such as around 70 s when the loading rate gradually increases, reaching its maximum around 120 s. The values of EMR and AE also increase accordingly, reaching their maximum. Between 120 s and 270 s, EMR and AE signals gradually weaken with the increasing stress. This is because, in the initial stage, the coal matrix has larger internal pores, and the coal matrix is compacted. During this stage, the compression of pores is greater than the compression of the coal matrix framework. As the pressure increases, the degree of compression decreases, and when it reaches approximately 270 s, the compression of pores in the coal matrix reaches its maximum, resulting in a lower value of EMR and AE signals. Subsequently, as the stress increases, the coal matrix framework begins to fracture under the load, and the degree of the coal matrix fracture gradually increases. At 650 s, the first significant fracture occurs, and the EMR signal suddenly intensifies. After the coal matrix fractures, the energy decreases, reaching its lowest point at 750 s. Since the coal matrix is in the experimental chamber and is subjected to a confining pressure, it does not become unstable. With the increasing pressure, the coal matrix fracture produces EMR and acoustic emission, and as the stress increases, the signal gradually strengthens, leading to another fracture. When it reaches 850 s, another fracture occurs. Afterward, despite the increasing pressure, there is no significant change in EMR energy of the coal matrix, indicating that the coal matrix has completely fractured, corresponding to a stress of 7 MPa. At the 20th minute, the stress level of the coal matrix no longer increases but remains at this pressure level, meaning the rate of force change is zero. It can be seen that both EMR energy and AE energy have reached lower values, and EMR and AE signals are consistent with the rate of force change.

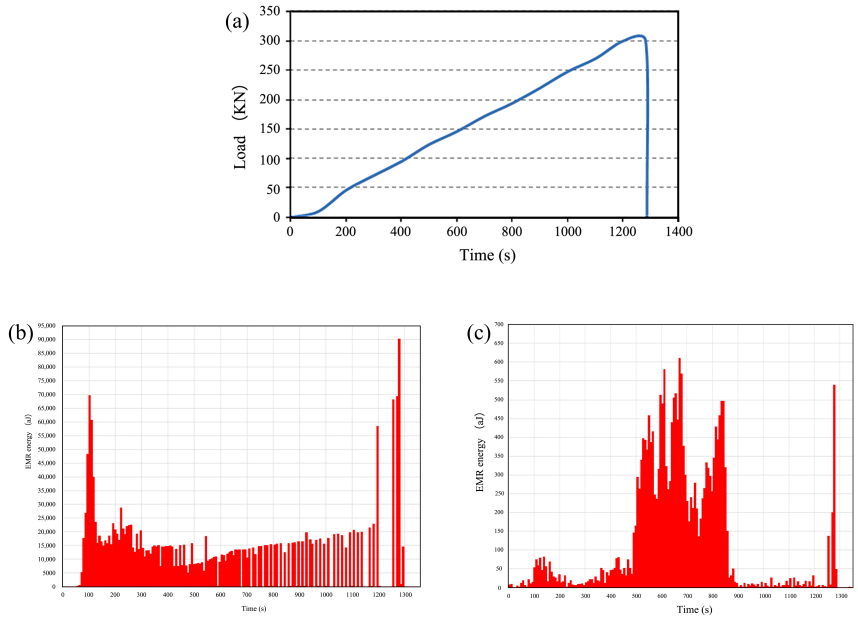


Figure 6. The acoustic–electric testing during the outburst process (0.32 MPa), Load curve (**a**), Channel 5 energy (**b**), Channel 6 energy (**c**).

Before a coal mine underground outburst occurs, there are usually variations in stress to some extent. EMR is a kind of electromagnetic wave energy radiated by the coal and rock mass in the process of uneven deformation under the action of load. The laboratory

research shows that high stress, crack propagation and gas flow cause the increase in EMR signals [24], which corresponds well with the outburst process of coal and gas. The EMR monitoring method can not only comprehensively characterize the gas, stress, coal-rock fracture process, and other information in front of the working face but also realize the continuous prediction of the evolution process in th coal and gas outburst there. In this section, the experiment tested the pattern of electrical potential signals in gas-bearing coal during the loading process. Overall, the trend in electrical potential signal changes is basically consistent with stress changes. As shown in Figure 7, at 380 s, a minor fracture occurred in the coal mass, and due to the fracture, free charges were generated, resulting in changes in various potential channels within the coal mass. Ch5, Ch2, and Ch12 all show varying degrees of increase. As the load continues to increase, the electrical potential signals in all channels change. Ch2 and Ch4 are both internal potentials of the coal matrix, and it can be seen that as the load increases during the loading process, the internal coal mass fracturing essentially ends, and the EP signals gradually decrease. Ch12, on the other hand, gradually strengthens with loading. Ch5, with load variations, does not show a very clear trend, but towards the end of the constant load phase, due to the change in the stress state, the signal in channel 5 decreases, and the rate of decrease gradually increases, which is related to the rapid reduction in stress. Ch3 is not far from Ch5 and both are on the outer surface of the coal matrix. Their trends are consistent, and during the constant load phase, the signal intensity decreases.

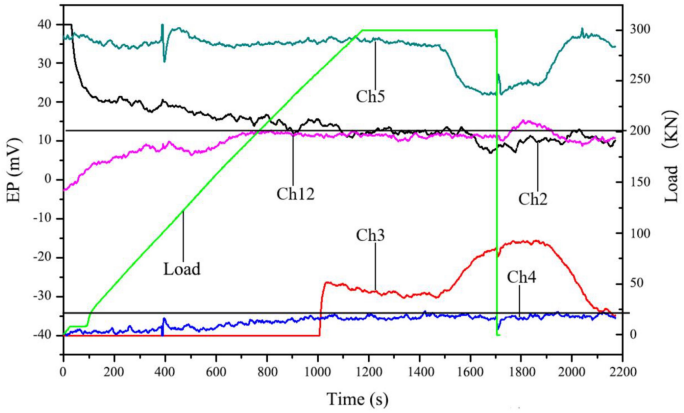


Figure 7. The results of EP signal testing during the coal and gas outburst process.

3.3. The Characteristics of the AE, EMR, and EP Signals during the Outburst Process

Coal and gas outbursts are rapid processes. During the outburst, the load suddenly decreases, gas rapidly escapes, and the coal is shattered and ejected. In coal mines, there are usually some precursors before a coal and gas outburst occurs. In this study, the changing patterns of acoustic–electric signals during the simulated underground roadway excavation process were tested. In Figure 8a represents the stress–strain of the coal, simulating the in situ stress at the site. Figure 8b–e represent EMR and AE signals during the simulated outburst process. Starting at 1444 s, the simulation of roadway excavation begins, and the outburst lasts for 3540 s. Figure 7b,c show the monitoring data for Channel 2 of the acoustic emission. From the figure, it can be seen that during the excavation process, as the roadway is excavated, the AE energy gradually increases. An obvious phenomenon can also be observed throughout the entire excavation process: it exhibits a certain periodic pattern. Within each periodic pattern, the variation shows a "peak" shape, where the values first increase and then decrease. Looking at the values of each period, there is a clear increasing trend. Starting from the fifth period, the magnitude of the AE signal enhancement becomes larger, and sudden signal clusters appear. At 3500 s, the length of the paraffin column reaches a critical value, and the frictional force between it and the borehole is not sufficient to maintain the original stress balance. As a result, sliding occurs, and the coal moves toward the outburst opening. As the coal unloads at the outburst opening, the AE signal

decreases and reaches a new equilibrium. As excavation continues, the length of the paraffin column becomes shorter, and its resistance to the outburst decreases. A larger sliding occurs, separating it from the coal. In front of the coal, the pressure is completely released from the geological stress, and the AE signal reaches a higher value. However, at this point, there is no widespread desorption of gas inside the coal. At 3540 s, the paraffin column is completely ejected, and the gas pressure inside the roadway suddenly drops to atmospheric pressure. Under a significant pressure difference, the gas inside the coal rapidly dissipates, and the coal is quickly shattered and pulverized, forming a coal and gas flow.

In Figure 8d,e represent Channel 5 for EMR signals. The figure shows that due to significant signal interference, the signal characteristics are not clearly evident during the excavation process.

In the simulation of roadway excavation, the paraffin column is relatively long, requiring a considerable amount of time for non-productive work. Through the analysis of Figure 8, it was found that this period has a relatively small impact on the coal body. In order to save experimental time and capture the acoustic–electric signals during the effective operation period, a method of shortening the paraffin column was adopted. The length of the paraffin column was adjusted based on the residual thickness of the paraffin column from the last outburst, with an additional safety thickness. Through calculations and empirical knowledge, the length of the paraffin column was ultimately reduced to 200 mm. After shortening the paraffin column, it can have an immediate impact on the coal in front of it once it is excavated or shortly after excavation.

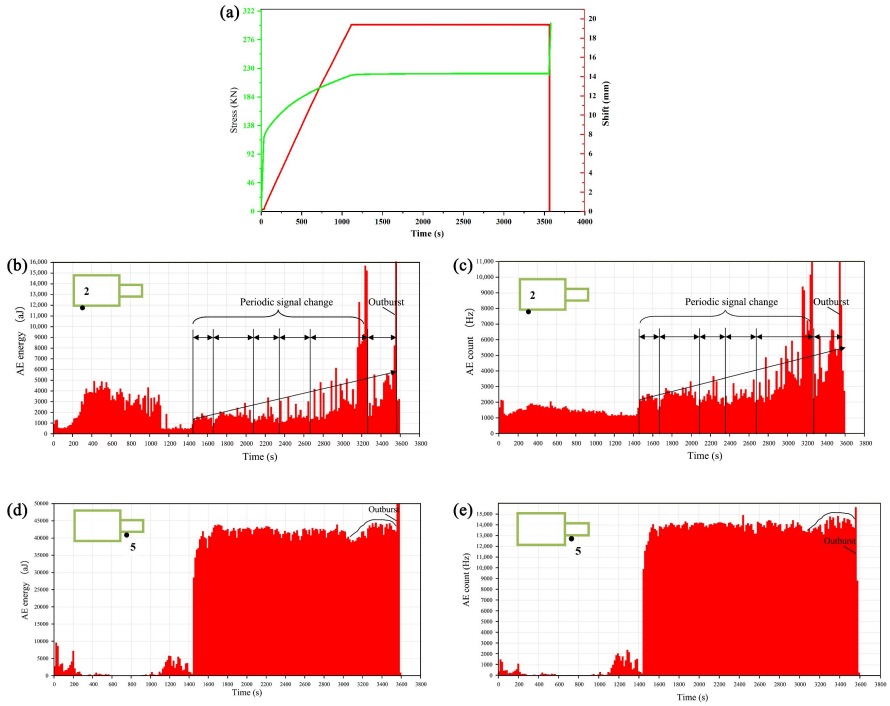


Figure 8. The acoustic–electric pattern testing during the outburst process, Stress–displacement curve (**a**), Channel 2 AE energy (**b**) and count (**c**), Channel 5 EMR energy (**d**) and count (**e**).

Figure 9b–e represent the energy and count signals of EMR Ch5 and Ch6. In the figure, the excavation point is at 1014 s. It can be seen from the figure that after the excavation "operation," the signal significantly increases. At 1130 s, the excavation operation affects the coal, causing the coal to fracture, releasing energy, and the system reaches a new balance with reduced signal intensity. As the operation progresses forward, the degree of coal fracture gradually increases. At 1550 s, the paraffin column slides towards the outburst opening and separates from the coal. The coal at the outburst opening expands

outward, partially releasing stress and reaching a new relative balance. The changes in stress have essentially disappeared, resulting in only slight changes in the coal mass, hence, the significant weakening of the EMR signal from the coal body. Subsequently, the paraffin column gradually moves towards the outburst opening, and at 1680 s, the paraffin column is completely ejected, exposing the coal wall entirely. Under a significant pressure difference, the coal and gas are ejected, completing the outburst. After the outburst, the geological stress no longer affects the coal, and the gas rapidly reaches atmospheric pressure. The disappearance of stress leads to a sharp drop in signal intensity. Looking at the data from Figure 8d,e, we find that they are similar in characteristics to the Channel 5 signal. However, their sensor placement is different from Channel 5, showing some differences, mainly in the following aspects: at the moment of sudden operation from the original system's stable equilibrium state, the EMR data signal has a high intensity; the outburst does not occur at the time of the strongest signal but during the process of signal reduction; generally, there is a "peak" appearing before the outburst. The reason for this peak is that the paraffin column moves under stress, the coal unloads and shatters, and the acoustic–electric signal intensifies. After the outburst, the signal drops sharply.

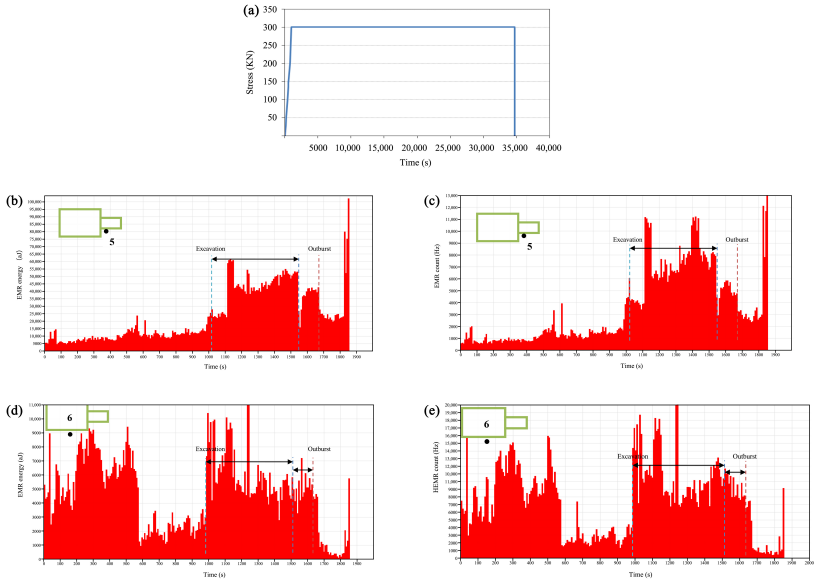


Figure 9. The acoustic–electric pattern testing during the roadway excavation process: Load curve (**a**), Channel 5 EMR energy (**b**) and count (**c**), Channel 6 EMR energy (**d**) and count (**e**).

In this set of experiments, the potential sensors in Ch5, Ch2, Ch4, and Ch11 are located on the same straight line as the outburst opening, with Ch11 channel being close to the outburst opening. Ch3, Ch6, Ch7, and Ch8 are close to the cylinder wall. The experiment was conducted at a gas pressure of 0.32 MPa, and the results are shown in Figure 10.

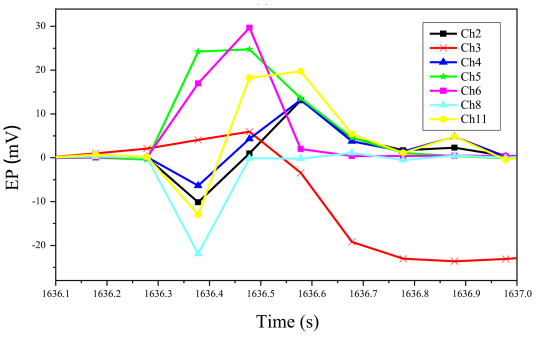


Figure 10. The characteristics of EP signal strength at the moment of outburst (0.32 MPa).

From the experimental results, it can be observed that there is a drastic change in the internal potential of the coal body at the moment of induced protrusion, with significant fluctuations. Among them, Ch2, Ch4, and Ch11 are internal potentials, located on the same line as the protrusion outlet, with Ch11 closest to the protrusion outlet, followed by Ch4 and Ch2. In terms of the trend in changes, the patterns of variation for the three channels are essentially consistent. The EP values rapidly decrease and then sharply increase at the moment of protrusion. During the rising phase, there are differences among the three, with the increase in Ch11 divided into two stages, the first stage being steeper and the second stage being more gradual. Ch2 and Ch4 both rise directly to their maximum values. This might be because Ch11 is near the outburst mouth, and the emission of all gas and coal during the protrusion process causes changes in the EP near Ch11, hence, the differences in the patterns of change. Furthermore, the amplitude of fluctuation is also different among the three, with the rising amplitude of Ch2, Ch4, and Ch11 being 20 mV, 17 mV, and 30 mV, respectively. Subsequently, the potential values decrease and gradually stabilize. Ch5 and Ch6 represent surface potentials, both located at the rear of the coal body, with their patterns of variation essentially consistent. The potential values rise rapidly and then decrease at the moment of protrusion. The patterns of change for these two channels are also not exactly the same. Ch5 and Ch6 can be divided into two stages, with Ch5 being more apparent and similar to the rising stage of Ch11. This might be because Ch5 and Ch6 are further from the protrusion outlet. In the initial stage of protrusion, the main factor is the gas desorption flow, causing coal body deformation and damage, and later, the coal body is ejected by high-pressure gas, resulting in the two-stage change in the potential of Ch5 and Ch6 channels. The rising amplitude is also different between the two, with ch5 and ch6 rising by 25 mV and 28 mV, respectively. Afterward, the three gradually stabilize. The Ch3 is also a surface potential, with the potential value slowly rising and then rapidly falling at the moment of protrusion. The potential value of the Ch8 channel rapidly decreases and then rapidly increases at the moment of protrusion, but after rising, the potential is level with the original potential value, with the subsequent changes in potential being stable and fluctuations being small.

The change in EP signal is a reflection of the internal damage and destruction of the coal body. The differences in the trajectories of EP signal changes indicate that there are variations in the damage and destruction of the coal body near each electrode slice. As analyzed and studied from Figure 10, showing the changes in EP signal at the moment of protrusion under gas pressure, it is known that during the protrusion process, the trend in internal potential change is that the potential value first decreases at the time of protrusion and then rapidly rises. The reason for the decrease is as follows: after the protrusion outlet opens, the stress in the coal body is released, and the gas is discharged. Subsequently, with the development of the coal body protrusion, a large amount of coal breaks, and the breaking of the coal body is accompanied by the separation of charges. The electrons with negative points escape, leaving only positive charges, leading to an increase in potential where the protrusion has occurred. As for the potential at the surface of the coal body, due to the discharge of coal and gas from the protrusion outlet during the protrusion process, accompanied by the rapid discharge of gas and the breaking of the coal body, charge separation occurs, leading to an increase in the EP signal at this location.

During the moment of induced protrusion, the potential values obtained from the tests undergo drastic changes, indicating that the coal body experiences internal ruptures due to the combined effects of gas and stress at this instant. The protrusion process is characterized by the release of the elastic potential energy of the coal body and the internal energy of the gas. The release of the coal elastic potential energy is inherently a process of damage and rupture. Thus, during the outburst of the coal body, the rapid expansion of fractures in the coal body generate a large number of free charges, leading to a rapid change in potential values. The release of gas internal energy is essentially a process where the non-equilibrium gas acts on the coal body. At the moment of induced protrusion, a significant gas pressure gradient is formed near the protrusion opening, and gas rapidly

flows towards the lower pressure side. Due to the brevity of this moment, the high-pressure gas exerts considerable force on the coal body, generating tensile stress within the coal body, leading to the rupture of the coal body near the opening and the outburst of gas. As a large amount of gas outbursts, internal fractures in the coal body extend along the existing "weak planes," separating out free charges and providing a pathway for the gas outburst. Hence, during the simulated protrusion, Ch2, Ch4, and Ch11, which are in a straight line with the protrusion opening, exhibit a significant gas pressure gradient, and their gradient directions are basically consistent, showing similar charge generation mechanisms and change patterns at the moment of protrusion. Potential test points far from the induced protrusion opening primarily participate in the protrusion process in the initial stage due to the rapid desorption and outward migration of adsorbed gas, continuously supplying gas for the protrusion. This process causes deformation of the coal body skeleton, leading to drastic changes in potential. When the gas pressure gradient and stress are sufficient to cause the coal body to rupture and be thrown out, the coal body and gas are expelled together.

The rupture of the coal body generates a large number of free charges, causing potential changes. Potential measurement points near the cylinder wall cannot provide high gas concentration, and the outburst is not as intense as at measurement points closer to the protrusion opening; thus, the induced potential change is not as strong. The high-speed outflow of gas causes a strong flow potential effect and triboelectricity, which is also one of the factors causing potential changes at the moment of outburst.

In summary, considering the different AE, EMR, and EP signals in the three stages, it can be seen that during the adsorption process, the irregularity of AE signals is caused by the varying strengths throughout the coal mass. The process of gas adsorption can cause damage and deformation to the coal body, disrupting the original charge balance within it and resulting in noticeable changes in electric potential values. During the loading process, the trends in AE, EMR, and EP signals are generally consistent with changes in stress. At the moment of outburst, as the coal and gas erupt, the AE and EMR signals increase sharply. Outbursts generally occur during the signal decline of AE and EMR, with the internal EP signal strength first decreasing and then rapidly rising. These findings suggest that there might be possible synergistic or correlated behaviors among EMR, AE, and EP signals. The difficulty and accuracy of monitoring signal changes vary at different stages. Therefore, the combined use of EMR-AE-EP signals for early warning can be used to enhance safety in coal mine production. However, our study was only conducted under simulated laboratory conditions, lacking field data. Additionally, these signals were not integrated, making them unsuitable for direct application. Utilizing machine learning methods to organize the data might provide more accurate and earlier warnings of coal and gas outburst.

4. Conclusions

For the on-site application of acoustic–magnetic–electric monitoring and early warning for coal and gas outbursts, a more comprehensive theoretical basis and experimental foundation are provided. The experiment studied the characteristics and laws of AE, EMR, and EP signals during the whole process of gas adsorption, stress loading, and outburst. The main conclusions of our work are as follows.

(1) This work analyzes the characteristics and patterns of AE, EMR, and EP signals during the adsorption process. During the gas adsorption process, the EMR signal changes with the coal mass gas adsorption pressure. A larger value of EMR appears at the initial moment of gas injection, then the value of EMR decreases rapidly; as gas injection proceeds, EMR intensity slowly rises, reaching its maximum value at 700 s, after which the signal intensity steadily decreases and remains constant after dropping to a certain value. The AE signal exhibits a trend opposite to that of the EMR signal, always showing an increasing trend. Moreover, the trend in EP signals varies

at different distances from the outburst outlet, and there are differences between the EP signals inside the coal mass and on its surface.

(2) The AE and EMR signals are consistent with the load change rate during the loading process. Overall, the intensities of both the AE signals and the EMR signals increase with the increase in stress.

(3) At the moment of an outburst, coal and gas erupt, resulting in a sharp increase in AE signals. Outbursts generally occur during the process of a decrease in AE and EMR signals. During the outburst, the internal EP signal intensity first decreases and then rapidly increases, while the surface EP signal intensity directly rises; the closer to the outburst mouth, the larger the amplitude change.

Author Contributions: Conceptualization, J.O. and E.W.; software, J.O.; writing—original draft preparation, J.O.; project administration, E.W. and Z.L.; investigation, J.O., N.L. and H.L.; writing—review and editing, J.O., H.L. and X.W. All authors have read and agreed to the published version of the manuscript.

Funding: This work was supported by the National Natural Science Foundation of China (No. 51974305) and the National Key R&D Program of China (2022YFC3004705).

Institutional Review Board Statement: Not applicable.

Informed Consent Statement: Not applicable.

Data Availability Statement: The data will be made available on request.

Conflicts of Interest: The authors declare no conflict of interest.

References

1. Liu, H.; Li, X.; Yu, Z.; Tan, Y.; Ding, Y.; Chen, D.; Wang, T. Influence of hole diameter on mechanical properties and stability of granite rock surrounding tunnels. *Phys. Fluids* **2023**, *35*, 064121.
2. Ren, F.; Zhu, C.; He, M.; Shang, J.; Feng, G.; Bai, J. Characteristics and precursor of static and dynamic triggered rockburst: Insight from multifractal. *Rock Mech. Rock Eng.* **2023**, *56*, 1945–1967. [CrossRef]
3. Li, H.; Li, X.; Fu, J.; Zhu, N.; Chen, D.; Wang, Y.; Ding, S. Experimental study on compressive behavior and failure characteristics of imitation steel fiber concrete under uniaxial load. *Constr. Build. Mater.* **2023**, *399*, 132599. [CrossRef]
4. Aguado, M.B.D.; Nicieza, C.G. Control and prevention of gas outbursts in coal mines, Riosa–Olloniego coalfield, Spain. *Int. J. Coal Geol.* **2007**, *69*, 253–266. [CrossRef]
5. Skochinski, A. Communication of the initiation of a sudden outburst of gas and coal in the model in outburst laboratory of the Institute of Mining of AN SSSR. *Ugol* **1953**, *10*, 39.
6. Ma, Y.-K.; Nie, B.-S.; He, X.-Q.; Li, X.-C.; Meng, J.-Q.; Song, D.-Z. Mechanism investigation on coal and gas outburst: An overview. *Int. J. Miner. Metall. Mater.* **2020**, *27*, 872–887. [CrossRef]
7. Wang, C.; Cheng, Y. Role of coal deformation energy in coal and gas outburst: A review. *Fuel* **2023**, *332*, 126019. [CrossRef]
8. Yin, D.; Chen, S.; Ge, Y.; Liu, R. Mechanical properties of rock–coal bi-material samples with different lithologies under uniaxial loading. *J. Mater. Res. Technol.* **2021**, *10*, 322–338. [CrossRef]
9. Chen, S.; Zhang, J.; Yin, D.; Li, F.; Lu, J.; Zhu, P. Visualizing Experimental Investigation on Gas–Liquid Replacements in a Microcleat Model Using the Reconstruction Method. *Deep. Undergr. Sci. Eng.* **2023**, *2*, 295–303. [CrossRef]
10. Qiu, L.; Zhu, Y.; Song, D.; He, X.; Wang, W.; Liu, Y.; Xiao, Y.; Wei, M.; Yin, S.; Liu, Q. Study on the nonlinear characteristics of EMR and AE during coal splitting tests. *Minerals* **2022**, *12*, 108. [CrossRef]
11. Zhou, B.; Xu, J.; Peng, S.; Yan, F.; Gao, Y.; Li, Q.; Cheng, L. Effects of geo-stress on the dynamic response of multi-physical field parameters during coal and gas outbursts under true triaxial stress. *Int. J. Rock Mech. Min. Sci.* **2021**, *142*, 104759. [CrossRef]
12. Soleimani, F.; Si, G.; Roshan, H.; Zhang, Z. Numerical modelling of coal and gas outburst initiation using energy balance principles. *Fuel* **2023**, *334*, 126687. [CrossRef]
13. Yin, G.; Jiang, C.; Wang, J.; Xu, J.; Zhang, D.; Huang, G. A new experimental apparatus for coal and gas outburst simulation. *Rock Mech. Rock Eng.* **2016**, *49*, 2005–2013. [CrossRef]
14. Li, J.; Hu, Q.; Yu, M.; Li, X.; Hu, J.; Yang, H. Acoustic emission monitoring technology for coal and gas outburst. *Energy Sci. Eng.* **2019**, *7*, 443–456. [CrossRef]
15. Wu, Y.; Li, W. Study on technology of electromagnetic radiation of sensitive index to forecast the coal and gas hazards. *Procedia Eng.* **2010**, *7*, 327–334. [CrossRef]
16. Zhang, X.; Tang, J.; Yu, H.; Pan, Y. Gas pressure evolution characteristics of deep true triaxial coal and gas outburst based on acoustic emission monitoring. *Sci. Rep.* **2022**, *12*, 21738. [CrossRef]

17. He, S.-Q.; Jin, L.-Z.; Ou, S.-N.; Ming, X.-H. Soft coal solid–gas coupling similar material for coal and gas outburst simulation tests. *J. Geophys. Eng.* **2018**, *15*, 2033–2046. [CrossRef]
18. Li, H.; Qiao, Y.; Shen, R.; He, M.; Cheng, T.; Xiao, Y.; Tang, J. Effect of water on mechanical behavior and acoustic emission response of sandstone during loading process: Phenomenon and mechanism. *Eng. Geol.* **2021**, *294*, 106386. [CrossRef]
19. Rabinovitch, A.; Frid, V.; Bahat, D. Directionality of electromagnetic radiation from fractures. *Int. J. Fract.* **2017**, *204*, 239–244. [CrossRef]
20. Qiu, L.; Li, Z.; Wang, E.; Liu, Z.; Ou, J.; Li, X.; Ali, M.; Zhang, Y.; Xia, S. Characteristics and precursor information of electromagnetic signals of mining-induced coal and gas outburst. *J. Loss Prev. Process. Ind.* **2018**, *54*, 206–215. [CrossRef]
21. Yang, H.; Wen, G.; Hu, Q.; Li, Y.; Dai, L. Experimental investigation on influence factors of acoustic emission activity in coal failure process. *Energies* **2018**, *11*, 1414. [CrossRef]
22. He, Y.; Zhao, P.; Li, S.; Ho, C.-H.; Zhu, S.; Kong, X.; Barbieri, D.M. Mechanical properties and energy dissipation characteristics of coal–rock-like composite materials subjected to different rock–coal strength ratios. *Nat. Resour. Res.* **2021**, *30*, 2179–2193. [CrossRef]
23. Dazhao, S.; Xueqiu, H.; Linming, D.; Ziyin, Z.; Anhu, W.; Zhenlei, L. Research on MS regional detection technology for coal and gas outburst hazard. *China Saf. Sci. J.* **2021**, *31*, 89.
24. Ren, F.; Zhu, C.; Yuan, Z.; Karakus, M.; Tang, S.; He, M. Recognition of shear and tension signals based on acoustic emission parameters and waveform using machine learning methods. *Int. J. Rock Mech. Min. Sci.* **2023**, *171*, 105578. [CrossRef]
25. Yin, Q.; Wu, J.; Zhu, C.; Wang, Q.; Zhang, Q.; Jing, H.; Xie, J. The role of multiple heating and water cooling cycles on physical and mechanical responses of granite rocks. *Geomech. Geophys.-Geo-Energy-Geo-Resour.* **2021**, *7*, 69. [CrossRef]
26. He, S.; Qin, M.; Qiu, L.; Song, D.; Zhang, X. Early warning of coal dynamic disaster by precursor of AE and EMR" quiet period". *Int. J. Coal Sci. Technol.* **2022**, *9*, 46. [CrossRef]
27. Shu, L.; Liu, Z.; Wang, K.; Zhu, N.; Yang, J. Characteristics and classification of microseismic signals in heading face of coal mine: Implication for coal and gas outburst warning. *Rock Mech. Rock Eng.* **2022**, *55*, 6905–6919. [CrossRef]
28. Liu, T.; Lin, B.; Fu, X.; Gao, Y.; Kong, J.; Zhao, Y.; Song, H. Experimental study on gas diffusion dynamics in fractured coal: A better understanding of gas migration in in-situ coal seam. *Energy* **2020**, *195*, 117005. [CrossRef]
29. Song, D.; Liu, X.; He, X.; Nie, B.; Wang, W. Investigation on the surface electrical characteristics of coal and influencing factors. *Fuel* **2021**, *287*, 119551. [CrossRef]
30. Qiu, L.; Song, D.; Li, Z.; Liu, B.; Liu, J. Research on AE and EMR response law of the driving face passing through the fault. *Saf. Sci.* **2019**, *117*, 184–193. [CrossRef]
31. Yang, C.; Liu, S.; Liu, J.; Yang, H.; Xie, J. Characteristics of self-potential of coal samples under uniaxial compression. *J. Appl. Geophys.* **2019**, *168*, 1–11. [CrossRef]
32. Zang, Z.; Li, Z.; Zhao, E.; Kong, X.; Niu, Y.; Yin, S. Electric potential response characteristics and constitutive model of coal under axial static load–dynamic load coupling. *Nat. Resour. Res.* **2023**, 1–24. [CrossRef]
33. Yuan, L. Control of coal and gas outbursts in Huainan mines in China: A review. *J. Rock Mech. Geotech. Eng.* **2016**, *8*, 559–567. [CrossRef]
34. Peng, S.; Zuo, S.; Wu, G.; Wang, C.; Liao, Y.; Tian, F. Research status and trend of coal and gas outburst: A literature review based on VOSviewer. *Int. J. Oil, Gas Coal Technol.* **2023**, *33*, 248–281. [CrossRef]
35. Niu, Y.; Wang, C.; Wang, E.; Li, Z. Experimental study on the damage evolution of gas-bearing coal and its electric potential response. *Rock Mech. Rock Eng.* **2019**, *52*, 4589–4604. [CrossRef]
36. Li, H.; Qiao, Y.; He, M.; Shen, R.; Gu, Z.; Cheng, T.; Xiao, Y.; Tang, J. Effect of water saturation on dynamic behavior of sandstone after wetting-drying cycles. *Eng. Geol.* **2023**, *319*, 107105. [CrossRef]
37. Li, H.; He, M.; Qiao, Y.; Cheng, T.; Xiao, Y.; Gu, Z. Mode I fracture properties and energy partitioning of sandstone under coupled static-dynamic loading: Implications for rockburst. *Theor. Appl. Fract. Mech.* **2023**, *127*, 104025. [CrossRef]
38. Yin, Q.; Wu, J.; Zhu, C.; He, M.; Meng, Q.; Jing, H. Shear mechanical responses of sandstone exposed to high temperature under constant normal stiffness boundary conditions. *Geomech. Geophys.-Geo-Energy-Geo-Resour.* **2021**, *7*, 1–17. [CrossRef]
39. Sobczyk, J. The influence of sorption processes on gas stresses leading to the coal and gas outburst in the laboratory conditions. *Fuel* **2011**, *90*, 1018–1023. [CrossRef]

Disclaimer/Publisher's Note: The statements, opinions and data contained in all publications are solely those of the individual author(s) and contributor(s) and not of MDPI and/or the editor(s). MDPI and/or the editor(s) disclaim responsibility for any injury to people or property resulting from any ideas, methods, instructions or products referred to in the content.